



## Synthesis of rGO-like materials from local agricultural wastes by microwave treatment followed by pyrolysis

Mona M. Rizk<sup>(1)</sup>, Mohamed S. Mahmoud<sup>(2)</sup>, N.M.Elzahid<sup>(3)</sup>, Ibrahim Ashour<sup>(4)</sup>

Department of Chemical Engineering, Faculty of Engineering, Minia University, El-Minya, Egypt<sup>(1)</sup>

Department of Chemical Engineering, Faculty of Engineering, Minia University, El-Minya, Egypt.  
Department of Engineering, University of Technology and Applied Sciences, Suhar, 311, Sultanate of Oman. <sup>(2)</sup>

Department of Chemical Engineering, Faculty of Engineering, Minia University, El-Minya, Egypt<sup>(3)</sup>

Department of Chemical Engineering, Faculty of Engineering, Minia University, Egypt <sup>(4)</sup>

\* Corresponding author. Tel.: +201016499917; email: [eng.mona.rizk@gmail.com](mailto:eng.mona.rizk@gmail.com).

### Abstract

In this work, we have synthesized multilayer rGO-like sheets from agricultural wastes. They have been successfully prepared from sugarcane bagasse, wheat straw, and peanut shell. The process involved using simple alkaline microwave treatment process followed by calcination under vacuum condition. The produced rGO-like material has been characterized by several analytical techniques like SEM, EDX, TEM, FTIR and XRD. These analysis confirmed formation of multilayer rGO-like sheets. These rGO-like sheets shows efficient activity as a photocatalyst for water splitting reaction under visible light radiation. The experimental results indicated that treatment of the wheat stalk by microwave in 3.0 M KOH solution at for 24 minutes and calcined the obtained solid at 800 °C under vacuum results in obtaining the maximum hydrogen production rate; 46.62 mmol H<sub>2</sub>/hr g<sub>cat</sub>. This is corresponding to solar-to-hydrogen conversion efficiency of 4.9 %. This study presents a new strategy for preparation of valuable photocatalysts from biomass wastes to be exploited green hydrogen production by photocatalytic water splitting under visible light radiation.

**Key words:** Wheat straw, bagasse pith, peanut shell, reduced graphene oxide-like, H<sub>2</sub> production.

## Introduction

Agricultural residues are being considered as one of the challenges that should be addressed to alleviate their adverse impact on the environment [1]. Instead of conventional disposal methods, researchers have focused on converting them into a valuable product. Graphene family is one of the proposed valuable products out of agricultural residues [1, 2]. Graphene is the thinnest type of smart material compared to the others. Andre Geim and Konstantin Novoselov developed graphene materials at the University of Manchester, and their outstanding achievements were honored with the Nobel Prize in 2010 [3]. Since then, it has become increasingly popular in human society, making it one of the most amazing scientific and technological accomplishments [4]. Due to the extremely tight or compact packing of atoms in the crystal lattice of graphene and its related compounds, graphene is one of the most stable materials [5, 6]. Graphene's fundamental structure is a two-dimensional single layer of carbon atoms with  $sp^2$  bonds that are consistently produced in a hexagonal lattice. In terms of mechanical, electronic, thermal, barrier, optical, and chemical properties, graphene is regarded as a smart material because of its high surface area, excellent thermal conductivity, high electron mobility, high Young's modulus, excellent high light transmittance, chemical stability, and high level of transparency, among other qualities [7-9]. Because of the aforementioned characteristics, graphene has the potential to be a material used in a wide range of sophisticated applications, including medicine, energy, electronics, and many others [10, 11]. Although producing high-quality graphene by processes like mechanical exfoliation [12], epitaxial growth on SiC [13], or molecular beam assembly

[14], their complexity and high price still limit their use to niche markets.

Recently, scientists have shown keen interest in producing rGO/rGO-like materials from agricultural waste. For instance, Makabodee Ruaysapa, et al. [15] studied the possibility of graphene production from coconut shell and cricket legs by chemical vapor deposition (CVD) and after characterization they found that graphene was synthesized from these materials in a multilayer structure. Dessy Ariyanti, et al. [16] studied the production of rGO-like materials from biomass; namely sugarcane bagasse, rice husk, coconut shell, and sawdust to be used for wastewater treatment. They used modified hammer's method for such synthesis and found that the prepared materials could follow even rGO patterns or graphene patterns. Several routes have been utilized to produce rGO/rGO-like materials and composites. For example, routes like CVD [15], hammers method [16], modified hammer's method [17], single step reforming [18], and sol-gel technique with mechanical ultracentrifugation [19], have been reported for such synthesis. Despite the advantages of these routes for production of rGO-like materials, little work has been done for synthesis of rGO like materials using microwave followed by calcination step. Therefore, this work was devoted to investigating a simple approach for preparing rGO-like materials using different types of agricultural wastes. Then, the synthesized materials have been characterized to figure out their components and structure. Later, each sample of the prepared rGO is used in photon-induced water splitting for  $H_2$  production and the results are displayed in detail. In this work, wheat straw, bagasse, and peanut shells have been used as agricultural stocks. Wheat straw is a by-product obtained after harvesting of wheat

grains and has an annual global production of about 529 million tons [20]. Wheat straw is composed of cellulose (34–40%), hemicellulose (20–25%), and lignin (20%). Sugar cane residues include bagasse and leaves, which are generated after the extraction of sugar from sugar cane stalks. Bagasse is the fibrous material that remains after crushing the stalks, while leaves are the green biomass that covers the stalks. It has a high content of cellulose (40–50%), hemicellulose (20–30%), and lignin (15–25%). Peanut shell is the outer covering of peanut seeds and accounts for about 25–30% of the total peanut weight. Peanut shell has a high content of lignin (28–36%), cellulose (25–35%), and hemicellulose (18–24%).

Photocatalytic water splitting is a process where the solar photons induce several reaction steps that result in production of both hydrogen and oxygen. Typically, titanium-based compounds are employed as a suitable photocatalysts for water photo-splitting [21]. Moreover, doping  $\text{TiO}_2$  with other elements also showed good catalytic toward this hydrogen producing reaction such Zn, Ni, Co, and Fe [22-29]. Likewise, rGO and rGO-like materials can induce the same reactions due to the presence of functional groups over the surface of these materials [30, 31]. Therefore, agricultural wastes can be a suitable stock to synthesize effective photocatalyst materials for hydrogen production process.

## 1. Experimental work

### 1.1. Chemicals and materials

Figure 1 shows a brief description of the experimental scheme followed in this study.

Hydrochloric acid (HCl, Loba Chemie) with 35-38% concentration is used in washing the raw material to remove any impurities on its surface. The agricultural feed stocks used are wheat straw, bagasse, and peanut shells. They have been crushed, grounded to an average aspect ratio of 1.0-1.2, and cleaned by soaking in HCl followed by drying at 60°C for 24 hr. Potassium hydroxide (KOH) is used in preparing a 3 M KOH solution to use it in the microwave treatment step. Distilled Water is used in filtration, preparing solutions and in washing through all the steps.

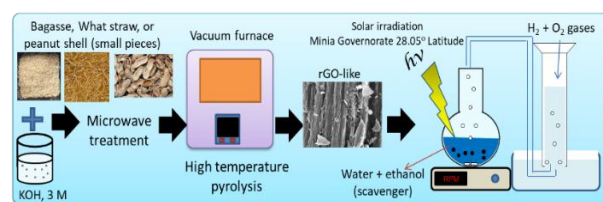


Fig. 1: experimental scheme used in this study.

## 2.2. Preparation of rGO-like materials using different agricultural wastes:

### 2.2.1. Preparation of raw materials

Few-layer graphene was produced from solid waste materials like wheat straw, peanut shell and sugar cane bagasse by two stages: carbonization and graphitization. Initially, the raw material was prepared by cutting into small pieces which were approximately 3 cm. and washed with distilled water, and then dried at 60°C for 12 hours.

### 2.2.2. Microwave treatment

In the microwave treatment, 4 gm of the raw material were submerged in 280 mL of homogeneous 3.0 M KOH solution in a microwave oven for 24 min

and then were left to cool down to room temperature naturally. The samples were collected by vacuum filtration, washed by 120 ml of distilled water for 30 min with stirring at room temperature, and then dried at 80 °C for 12 hours.

### 2.2.3. High temperature pyrolysis

The samples were heated in a tubular furnace at 800 °C for 3 hours under vacuum. This is done to chemically activate the prepared samples by the high temperature pyrolysis. Later, the carbonaceous samples were washed with 0.5 M HCl solution to remove the residual KOH and dried in a vacuum oven at 80 °C for 12 hours.

### 2.2.4. photocatalytic water splitting

The experiment was conducted in a 250 ml conical flask, where 50 mg of the rGO-like photocatalyst was added to an aqueous solution of water and methanol (75 ml water: 25 ml methanol) to split water/methanol over the photocatalysis using solar photons. The sample was stirred to promote gas detachment during the reaction by reducing the hydrodynamic boundary layer around each photocatalyst particle. The O<sub>2</sub>/H<sub>2</sub> gases were collected above the water in an overturned graduated cylinder, and the volume of accumulated hydrogen was calculated by measuring the rate of volume increase over time. The experiments were conducted under solar irradiation from 12:00~13:00 in July 2021 in Minia City, Egypt (Latitude: 28° 06' 35.6" N Longitude: 30° 45' 1.1" E) on consecutive days at a fixed time to minimize the effect of solar radiation fluctuations.

## 2. Results and discussion

The prepared rGO-like samples have been characterized by different characterization techniques to figure out their structure and components.

### 3.1 X-ray diffraction (XRD):

XRD have been performed for the samples to discover their crystal structure. The crystalline structure of the sample made from wheat straw is shown in Fig. 2. It's clear that there are 2 strong peaks at 2θ values 24.26 and 44 degrees. This corresponds to the crystal plans of [0 0 2] and [1 0 0] of graphite obtained from carbon resources. This finding is in line with the data shown by B. Gupta et al. [32]. They indicated that if the samples contain crystalline graphite, the lattice spacing typically will be at 0.34 nm, while the lattice spacing increases in the presence of rGO due to the presence of oxygen functional groups. The peaks are not sharp due to the presence of multilayers of rGO nanosheets in the sample [33].

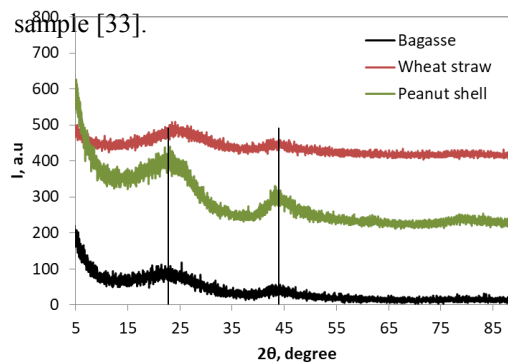


**Fig. 2:** the XRD results for the samples made from bagasse, wheat straw, and peanut shell

Figure 2 also represents the XRD pattern for the sample made from sugar cane bagasse. As being clear from the figure, there are 3 peaks at 2θ values 21.24,

42.56 and 22.26 and this means that the sample contains carbon in a crystalline shape including some impurities. Furthermore, the XRD result for the sample made from peanut shell is presented indicated that there are 3 peaks at  $2\theta$  values 22.90, 23.62 and 44.98 degrees. So, it contains carbon in crystal form. In the XRD figures, the full width at half maximum (FWHM) can be calculated. It represents the difference the intensity of the light at half of its maximum value. It represents the width of the XRD spectrum at half of the maximum amplitude. The FWHM for the XRD figure is typically used to identify the material properties and the surface structure of the prepared samples. It can give specific information about the lattice structure, phase, texture or the presence of stresses for the polycrystalline materials. Table 1 shows the values of FWHM for the three prepared samples. It has been calculated from the following formulae assuming Gaussian distribution.

$$f(x) = \frac{1}{\sigma\sqrt{2\pi}} \exp\left(-\frac{(x-x_0)^2}{2\sigma^2}\right) \quad (1)$$

where  $\sigma$  is the standard deviation,  $x_0$  is the expected  $x$  value. So, the FWHM is obtained from:

$$\text{FWHM} = 2\sqrt{2\ln 2}\sigma \approx 2.355\sigma$$

It is evident that the broadening in the peaks of the XRD patterns comes from the small size of the crystals. Larger are the crystal sizes, sharper will be the peaks in the XRD pattern whereas smaller crystal size will make the peak broader.

### 3.2 Scanning Electron Microscopy (SEM) with EDX Analysis:

The crystal morphology and sample analysis are obtained by using SEM/EDX analysis for the prepared samples. Figure 3 shows an image of the sample surface topography which made from sugar cane bagasse as a raw material in a magnification of  $5\mu\text{m}$ . It proves that the sample has relatively high surface area. Also, Figure 3 shows a detailed analysis for the sample components arranged from the highest concentration component to the least one and it's clear that the sample is almost composed of carbon. Also, trace elements like Mg, Si, Ca, and Cu appear in the sample. These trace elements typically appear in the bagasse as indicated by H. Hajiha and M.Sain [34]. Higher the value of the trace elements will make the bagasse more brittle. Figure 4 displays a magnified image ( $10\mu\text{m}$ ) for the sample made from wheat straw as a raw material, it shows that due to treatment, the surface becomes rough, soft and weak due to removal of lignin, pyrolysis of cellulose, and production of rGO. However, the fibers of wheat straw appear to maintain its arrangement even after treatment which means that subsequent step is necessary to produce rGO in a typical layer form. Likewise, Fig. 4 shows a detailed analysis for the sample components arranged from the highest concentration component to the least one and it's clear that the sample is almost composed of carbon. Other trace elements come from the residual lignin and other impurities. In Fig. 5, a magnified image of the sample made from peanut shell as a raw material is displayed to show the presence of scattered layered rGO particles appears over the substrate of the peanut shell after pyrolysis. Figure 5 also shows all the components of the sample starting from the highest concentration component. Traces of Mg, Ca, Cu and Zn are available in the peanut shell sample which is typically reported in the literature [35].

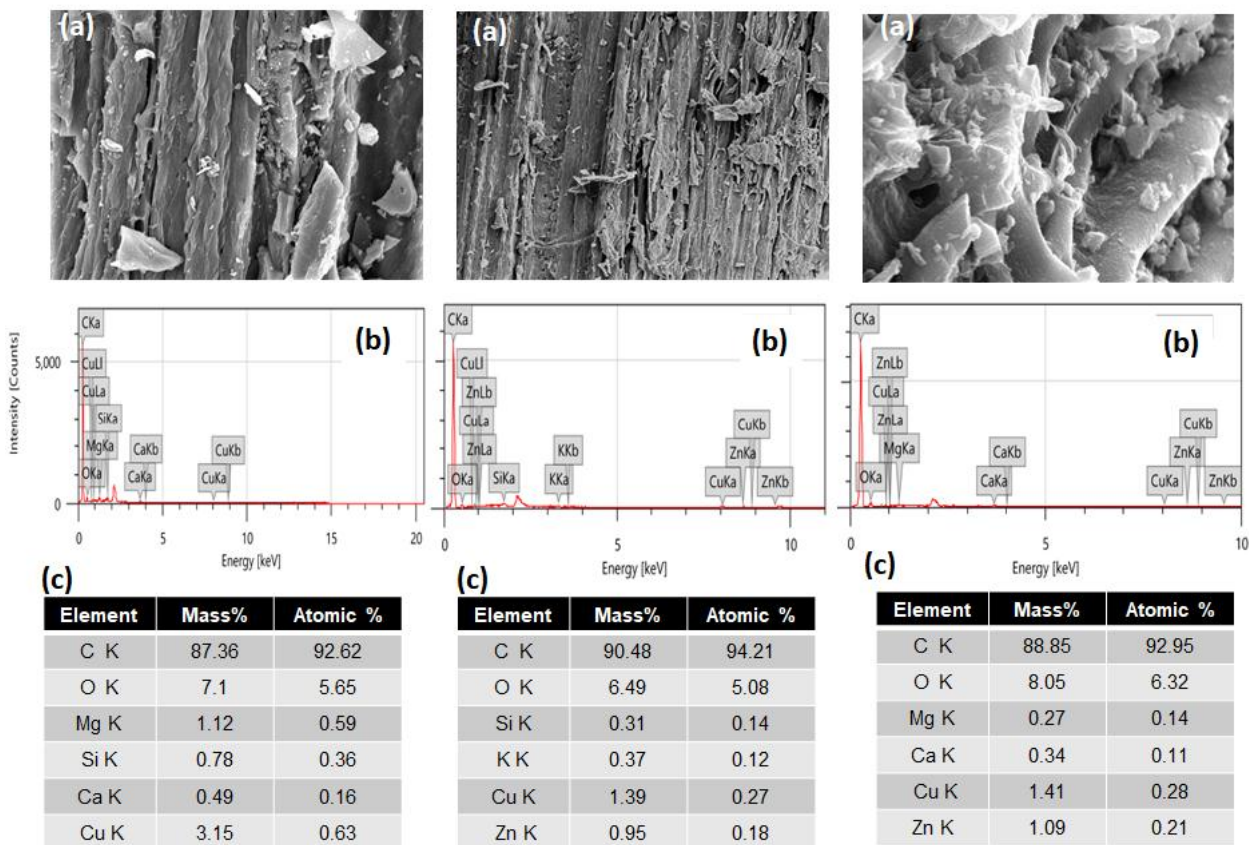


**Fig. 3 (a, b and c):** SEM with EDS analysis results for the samples made from bagasse pith.

**Fig. 4 (a, b and c):** SEM with EDS analysis results for the samples made from wheat straw.

**Fig. 5 (a, b and c):** SEM with EDS analysis results for the samples made from peanut shell.

### 3.3 TEM images:

Figure 6 shows the TEM images for the prepared samples. It is evidence that various morphologies of rGOs have been generated. The images reveal that all the as-prepared rGOs samples from the agricultural residues are in the sheet-like structure. However, the sheets are not as thin as the samples prepared by other methods. In fact, the gray color gradient at the sheets ends give an evident that the samples consist of a few layers of rGO sheets that stack together as explained by Hebat-Allah S., et al. [36].

**Table 1:** Raman spectroscopy and XRD data and related attributes of rGO

	Sugarcane bagasse		Wheat straw		Peanut shells	
	Raman shift (cm <sup>-1</sup> )	FWHM (cm <sup>-1</sup> )	Raman shift (cm <sup>-1</sup> )	FWHM (cm <sup>-1</sup> )	Raman shift (cm <sup>-1</sup> )	FWHM (cm <sup>-1</sup> )
D-band	1335.12	9.1	1346.48	12.455	1338.32	10.76
G-band	1589.88		1582.42		1597.93	
I <sub>D</sub> /I <sub>G</sub> ratio	1.03		1.09		0.93	

### 3.4 Raman spectroscopy:

Figure 7 displays Raman analysis results of the samples made from wheat straw, sugar cane bagasse and peanut shell. There are two peaks appeared representing the disordered (D) and graphitic (G) planes for all the three samples. The G band that should appear at around  $1590\text{ cm}^{-1}$  is obtained at  $1589.9$ ,  $1582.4$  and  $1597.9\text{ cm}^{-1}$  for sugar bagasse, wheat straw and peanut shell, respectively. It is obtained due to bond stretching at  $sp^2$  for the carbon pairs in the forms of both rings and chains, indicating the appearance of graphitic structure. Regarding the D band, the values were around  $1350\text{ cm}^{-1}$  as shown in Table 1. These values correspond to the presence of aromatic rings, representing some defects in the lattice structure due to the preparation process [37, 38]. The intensity of D band  $1350\text{ cm}^{-1}$  increases by increasing the amount of disorderly organized carbon in the three samples and also to a decrease in the size of the crystals [38]. A positive shift in frequency ( $\approx 15\text{ cm}^{-1}$ ) was observed in some samples with small crystal sizes. This band was attributed to  $E_{2g}$  mode of vibrations, which was restricted to the motion of atoms to the plane of the carbon atoms [39]. The intensity ratio of the (ID/IG) increases as the amount of disorder increases. This ratio is often used to determine the average size of crystal planar domains ( $L_a$ ) [40, 41]. Thus, the ratio of the peak's intensity of the ID/IG peak typically shows a clue for the degree of the disorder of the graphitization process. It is clear from Table 1 that the values of ID/IG are near each other, indicating the good degree of graphitization of the prepared samples. It is clear from our results that the most ordered crystals were for peanut shell and the highest disorder was for the wheat straw. This high disorder will provide more

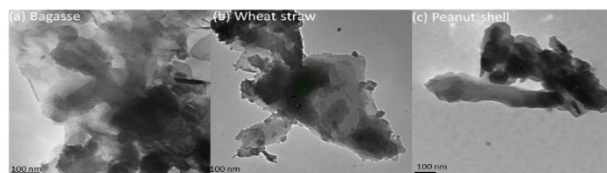


**Fig. 6 (a, b and c):** TEM images for (a) rGO prepared from Bagasse, (b) rGO prepared from active sites for hydrogen generation from water photo-splitting reactions.

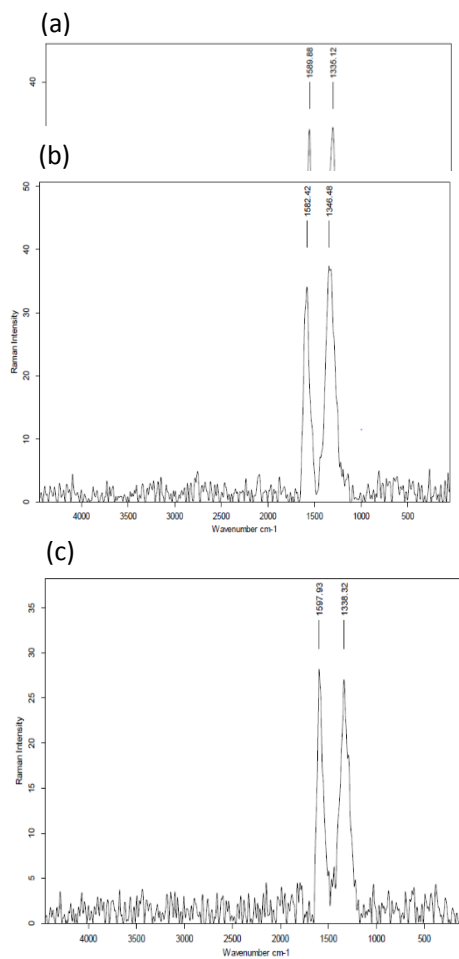


**Fig. 7:** Raman analysis of the sample made from (a) sugarcane bagasse, (b) Wheat straw and (c) peanut shells.

### 3.5 Utilization of the prepared samples in photon-induced water splitting

Figure 8 shows a typical time course for H<sub>2</sub> production using the prepared rGO-like photocatalyst under solar irradiation. It is evident that wheat straw catalyst produced the highest rate of H<sub>2</sub> production (46.62 mmol/h g catalyst), then it decreases for sugarcane bagasse and peanut shell samples as shown in Table 2. These results are in line with that obtained by Xiang, Q et al and Hager M et al [39, 42] who showed that rGO can induce the water splitting reaction over its surface due to the presence of oxygen-containing functional groups that facilitate charge separation and transfer. Furthermore, many workers indicated that rGO can act as p-type semiconductor [43, 44]. This is due to the presence of scattered C-O bonds over the surface of the rGO-like photocatalyst.

For the photocatalytic reactions, the size of the photocatalyst determines the rate of the photocatalytic reaction. Throughout the photocatalytic reactions of the photocatalyst, water split occurs due to both oxygen and hydrogen evolution reactions (OER and HER). The composition and size of the photocatalyst significantly affect the performance of the photocatalyst. It is clear that the activation energy is low for the photocatalytic reactions relative to actual reactions. However, the photocatalytic reactions usually undergo slowly due to the low activity, which in turn is due to the multi-electron transfer steps that happens for both the oxygen and hydrogen evolution reactions. It is reported by Wang Q. et al. [45] that the generation of oxygen occur on a second's scale, while the hydrogen reaction occurs 100,000 times faster

than the oxygen evolution reaction. This implies that the OER is the slowest step in the hydrogen generation from water splitting reactions.

Photocatalytic activity is strongly influenced by the optical properties of the light source used in experiments, such as light intensity and irradiation area. As a result, it is difficult to compare catalyst activities if the reaction conditions are different. It is therefore essential to determine the apparent quantum yield (AQY), which eliminates the effect of the light source, to compare the efficiency of the present system with other published works. The quantum efficiency of photocatalytic water splitting is calculated using the following equation:

$$\eta = \frac{n_e}{n_\nu} \quad (2)$$

where  $\eta$  here represents the energy conversion efficiency,  $n_e$  is the number of electrons exchanged in the hydrogen evolution reaction, and  $n_\nu$  is the number of photons reached the reaction area. The value of  $n_e$  can be obtained using the rate of hydrogen evolution from Table 2. 8 H<sub>2</sub> evolution rate was = 46.62 mmol H<sub>2</sub> g<sup>-1</sup> catalyst hr<sup>-1</sup> for wheat straw rGO photocatalyst. Using this rate, the electrons involved in the hydrogen evolution reaction can be calculated. Also, the  $n_\nu$  is calculated using the following equation:

$$N_\nu = \frac{I}{E_\nu} \quad (3)$$

where  $I$  is the intensity of solar irradiations measured for El Minia Governorate, Egypt (Latitude: 31° 25',

$I = 258\text{--}266.7 \text{ Wm}^{-2}$  [46]) and  $E_v$  is the photon energy ( $3.97 \times 10^{-19}$ , J photon<sup>-1</sup>). Hence, the intensity of the photon flux is calculated to equal  $6.51 \times 10^{20}$  photons/s m<sup>2</sup> solar. This calculation indicates that the prepared catalyst has achieved a 7.2 % conversion of photons to electrons, showing that this rGO-like photocatalyst can increase the absorbance of photons and prolong the lifetime for e/h pairs.

Researchers have also adopted a practical standard for calculating the efficiency of photocatalytic water splitting, known as solar-to-hydrogen (STH) efficiency, which can be determined using a specific formula:

$$STH = \frac{\text{Energy stored in } H_2 \text{ gas}}{\text{Incident solar energy}} = \frac{r_{H_2} \Delta G}{IA_r} \quad (4)$$

where  $r_{H_2}$  is the rate of hydrogen evolution in moles/sec,  $\Delta G$  is the Gibbs free energy for hydrogen gas in J/mol, and  $A_r$  is the apparent surface area of the reaction. Using this formula, the STH efficiency of the photocatalyst prepared from wheat straw is calculated to be 4.9%. Table 3 shows a comparison between the rate of hydrogen evolution for different photocatalysts. It is important to note that comparison of the rate of hydrogen evolution should be made for experiments that are conducted using the same light source and same sacrificing agent. However, it is hard to fulfill that condition to compare our results with other works. It is clear that the prepared photocatalyst is comparable to the work done by Hager et al. [42] but better than that prepared by Fang Liu et al. [53]. This discrepancy is due to the different

preparation techniques and different experimental parameters. Also, it is noticeable that addition of other nanoparticles doped to the rGO may also enhance the rate of hydrogen evolution as shown in the work of Babu SG, et al [51].

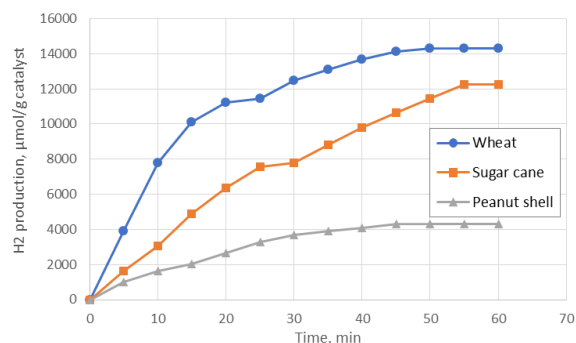


**Fig. 8:** Photocatalytic H<sub>2</sub> production rates for different prepared catalyst under solar irradiation

Table 2: Different concentration of catalyst in 100 mL of water/ethanol solution

Initial rate of H <sub>2</sub> evolution mmol/h g <sub>catalyst</sub>	H <sub>2</sub> evolution mmol/ g <sub>catalyst</sub>	Nanoparticle	Run no.
18.4	12.27	rGO/sugarcane bagasse	1
46.62	14.31	rGO/Wheat straw	2
9.82	4.3	rGO/peanut shell	3

**Table 3:** the rate of hydrogen production using different rGO-based photocatalysts.

Nanoparticles	Photons Source	Scavenger used	Rate of H <sub>2</sub> production	Reference/ date
rGO/TiO <sub>2</sub>	350-W Xe arc lamp	25% Methanol	0.736 mmol/h g	[47]/2011
rGO/TiO <sub>2</sub>	300 W Xe arc lamp	20% vol methanol	1.76 $\mu$ mol/h	[48]/2012
MoS <sub>2</sub> /rGO	300 W Xe arc lamp	15% (v/v) TEOA	83.8 $\mu$ mol/h	[49]/2012
rGO/TiO <sub>2</sub>	150 W Hg/Xe lamp	0.5 M Na <sub>2</sub> SO <sub>3</sub>	127.5 $\mu$ mole cm <sup>-2</sup> h	[31]/2014
rGO/TiO <sub>2</sub>	UV-light (365 nm, 3 W)	Na <sub>2</sub> S & Na <sub>2</sub> SO <sub>3</sub>	2 mmol/h g	[50]/2014
Cu <sub>2</sub> O/TiO <sub>2</sub> /rGO	250 W Xe arc lamp	5% glycerol	110.97 mmol/h g	[51]/2015
rGO/TiO <sub>2</sub>	300 W Xe lamp, $\lambda > 300$ nm	20 % vol. aqueous methanol	0.72 mmol/g-h	[52]/2017
rGO	Hg lamp	0.1 M Na <sub>2</sub> S and 0.04 M Na <sub>2</sub> SO <sub>3</sub>	17.18 mmol/h g catalyst	[36]/2022
rGO	UV-vis light	20 vol% Methanol	0.1 mmol/h g	[53]/2020
This work	Solar irradiation	Methanol	14.31 mmol/g catalyst	

### 3. Conclusion

Graphene, the thinnest material in the world, is synthesized by several methods. In this study, rGO-like photocatalyst has been prepared from different types of agricultural wastes: sugarcane bagasse, wheat straw and peanut shell through some steps started with cleaning the agricultural stock, thermal treatment in KOH, and high temperature pyrolysis in vacuum atmosphere. The prepared rGO-like samples have been characterized by different types of characterization, like XRD, SEM, EDS, TEM, and RAMAN as the results proved the formation of rGO-

like material consists of several layers of rGO. It was evident from RAMAN analysis that the most ordered crystals were obtained from the peanut shell and the highest disorder was for the wheat straw. This high disorder provided more active sites for hydrogen generation from water photo-splitting reactions. Finally, the prepared samples have been used in photon-induced water splitting For H<sub>2</sub> production where they showed that wheat straw catalyst produced the highest rate of H<sub>2</sub> production (46.62 mmol/h g<sub>catalyst</sub> with STH % of 4.9%), then it decreases for sugarcane bagasse and peanut shell samples. The prepared

### 4. References

- [1] B. P. Singh *et al.*, "Green and Sustainable Technology for Clean Energy Production: Applications," in *Handbook of Green and Sustainable Nanotechnology: Fundamentals, Developments and Applications*: Springer, 2023, pp. 1-23.
- [2] D. Anggoro, D. Ristiani, E. Widiyanto, I. Santoso, and G. Yudoyono, "Optical properties and defect states of rGO-like carbon derived from biomass with heating treatment," *Materials Chemistry and Physics*, vol. 303, p. 127795, 2023.
- [3] E. Gerstner, "Nobel prize 2010: Andre geim & konstantin novoselov," *Nature Physics*, vol. 6, no. 11, pp. 836-836, 2010.

- [4] S. K. Tiwari, V. Kumar, A. Huczko, R. Oraon, A. D. Adhikari, and G. Nayak, "Magical allotropes of carbon: prospects and applications," *Critical Reviews in Solid State and Materials Sciences*, vol. 41, no. 4, pp. 257-317, 2016.
- [5] S. K. Tiwari, R. K. Mishra, S. K. Ha, and A. Huczko, "Evolution of graphene oxide and graphene: from imagination to industrialization," *ChemNanoMat*, vol. 4, no. 7, pp. 598-620, 2018.
- [6] S. K. Tiwari, S. Sahoo, N. Wang, and A. Huczko, "Graphene research and their outputs: Status and prospect," *Journal of Science: Advanced Materials and Devices*, vol. 5, no. 1, pp. 10-29, 2020.
- [7] L. I. Silva, D. A. Mirabella, J. P. Tomba, and C. C. Riccardi, "Optimizing graphene production in ultrasonic devices," *Ultrasonics*, vol. 100, p. 105989, 2020.
- [8] J. Wei, R. Atif, T. Vo, and F. Inam, "Graphene nanoplatelets in epoxy system: dispersion, reaggregation, and mechanical properties of nanocomposites," *Journal of Nanomaterials*, vol. 16, no. 1, pp. 374-374, 2016.
- [9] J. Phiri, P. Gane, and T. C. Maloney, "General overview of graphene: Production, properties and application in polymer composites," *Materials Science and Engineering: B*, vol. 215, pp. 9-28, 2017.
- [10] S. Stankovich *et al.*, "Graphene-based composite materials," *nature*, vol. 442, no. 7100, pp. 282-286, 2006.
- [11] D. R. Dreyer, R. S. Ruoff, and C. W. Bielawski, "From conception to realization: an historical account of graphene and some perspectives for its future," *Angewandte Chemie International Edition*, vol. 49, no. 49, pp. 9336-9344, 2010.
- [12] K. S. Novoselov *et al.*, "Electric field effect in atomically thin carbon films," *science*, vol. 306, no. 5696, pp. 666-669, 2004.
- [13] P. Sutter, "How silicon leaves the scene," *Nature materials*, vol. 8, no. 3, pp. 171-172, 2009.
- [14] J. Park *et al.*, "Epitaxial graphene growth by carbon molecular beam epitaxy (CMBE)," *Advanced Materials*, vol. 22, no. 37, pp. 4140-4145, 2010.
- [15] M. Ruaysap, T. Pongphai, K. Sirilapphokhin, P. Sirilapphokhin, and U. Tipparach, "Synthesis of graphene from food and agricultural wastes in ubon ratchathani province, thailand," *Journal of Materials Science and Applied Energy*, vol. 11, no. 2, pp. 244465-244465, 2022.
- [16] D. Ariyanti, D. Lesdantina, A. Purbasari, and Y. Astuti, "Synthesis of graphene-like material derived from biomass from agricultural waste and its application in Cu (II) removal," *Korean Journal of Chemical Engineering*, vol. 40, no. 4, pp. 964-974, 2023/04/01 2023, doi: 10.1007/s11814-023-1380-8.
- [17] P. S. Selvamani, J. J. Vijaya, L. J. Kennedy, B. Saravanakumar, and M. Bououdina, "Microwave synthesized  $\alpha$ -Fe<sub>2</sub>O<sub>3</sub>/MoS<sub>2</sub>/rGO composites as high-performance supercapacitor," *Materials Letters*, vol. 293, p. 129721, 2021.
- [18] T. Somanathan, K. Prasad, K. Ostrikov, A. Saravanan, and V. Mohana Krishna, "Graphene oxide synthesis from agro waste," *Nanomaterials*, vol. 5, no. 2, pp. 826-834, 2015.
- [19] E. Suarso *et al.*, "Enhancement of LiFePO<sub>4</sub> (LFP) electrochemical performance through the insertion of coconut shell-derived rGO-like carbon as cathode of Li-ion battery," *Journal of Materials Science: Materials in Electronics*, vol. 32, no. 24, pp. 28297-28306, 2021/12/01 2021, doi: 10.1007/s10854-021-07206-5.
- [20] Y. Ma, Y. Shen, and Y. Liu, "State of the art of straw treatment technology: Challenges and solutions forward," *Bioresource Technology*, vol. 313, p. 123656, 2020/10/01/ 2020, doi: <https://doi.org/10.1016/j.biortech.2020.123656>.
- [21] E. Morais, C. O'Modhrain, K. R. Thampi, and J. A. Sullivan, "RuO<sub>2</sub>/TiO<sub>2</sub> photocatalysts prepared via a hydrothermal route: Influence of the presence of TiO<sub>2</sub> on the reactivity of RuO<sub>2</sub> in the artificial photosynthesis reaction," *J. Catal.*, vol. 401, pp. 288-296, 2021.
- [22] M. I. Díez-García and R. Gómez, "Investigating water splitting with CaFe<sub>2</sub>O<sub>4</sub> photocathodes by electrochemical impedance spectroscopy," *ACS Appl. Mater. Interfaces*, vol. 8, no. 33, pp. 21387-21397, 2016.
- [23] P. Sahoo, A. Sharma, S. Padhan, and R. Thangavel, "Visible light driven photosplitting of water using one dimensional Mg doped ZnO nanorod arrays," *Int. J. Hydrogen Energ.*, vol. 45, no. 43, pp. 22576-22588, 2020.
- [24] S. S. Arbuj, R. R. Hawaldar, S. Varma, S. B. Waghmode, and B. N. Wani, "Synthesis and characterization of ATiO<sub>3</sub> (A= Ca, Sr and Ba) perovskites and their photocatalytic activity under solar irradiation," *Science of Advanced Materials*, vol. 4, no. 5-6, pp. 568-572, 2012.

- [25] K. M. Kim, B. S. Kwak, S. Kang, and M. Kang, "Synthesis of submicron hexagonal plate-type SnS<sub>2</sub> and band gap-tuned Sn<sub>1-x</sub>Ti<sub>x</sub>S<sub>2</sub> materials and their hydrogen production abilities on methanol/water photosplitting," *International Journal of Photoenergy*, vol. 2014, 2014.
- [26] W. Septina, S. Ikeda, T. Harada, M. Higashi, R. Abe, and M. Matsumura, "Photosplitting of water from wide-gap Cu (In, Ga) S<sub>2</sub> thin films modified with a CdS layer and Pt nanoparticles for a high-onset-potential photocathode," *J Phys Chem C*, vol. 119, no. 16, pp. 8576-8583, 2015.
- [27] Y. Yang *et al.*, "Oxygen-vacancy-induced O<sub>2</sub> activation and electron-hole migration enhance photothermal catalytic toluene oxidation," *Cell Reports Physical Science*, vol. 3, no. 8, p. 101011, 2022.
- [28] M. S. Mahmoud, E. Ahmed, A. A. Farghali, A. H. Zaki, E. A. M. Abdelghani, and N. A. M. Barakat, "Influence of Mn, Cu, and Cd doping for titanium oxide nanotubes on the photocatalytic activity toward water splitting under visible light irradiation," *Colloids and Surfaces A: Physicochemical and Engineering Aspects*, vol. 554, pp. 100-109, 2018 2018, doi: 10.1016/j.colsurfa.2018.06.039.
- [29] M. S. Mahmoud, E. Ahmed, A. Farghali, A. Zaki, and N. A. Barakat, "Synthesis of Fe/Co-doped titanate nanotube as redox catalyst for photon-induced water splitting," *Materials Chemistry and Physics*, vol. 217, pp. 125-132, 2018.
- [30] N. A. M. Barakat *et al.*, "Distinct influence for carbon nano-morphology on the activity and optimum metal loading of Ni/C composite used for ethanol oxidation," *Electrochimica Acta*, vol. 182, pp. 143-155, 2015 2015, doi: 10.1016/j.electacta.2015.09.079.
- [31] P. K. Dubey, P. Tripathi, R. Tiwari, A. Sinha, and O. Srivastava, "Synthesis of reduced graphene oxide-TiO<sub>2</sub> nanoparticle composite systems and its application in hydrogen production," *international journal of hydrogen energy*, vol. 39, no. 29, pp. 16282-16292, 2014.
- [32] B. Gupta, N. Kumar, K. Panda, V. Kanan, S. Joshi, and I. Visoly-Fisher, "Role of oxygen functional groups in reduced graphene oxide for lubrication," *Scientific reports*, vol. 7, no. 1, pp. 1-14, 2017.
- [33] S. Pei and H.-M. Cheng, "The reduction of graphene oxide," *Carbon*, vol. 50, no. 9, pp. 3210-3228, 2012.
- [34] H. Hajiha and M. Sain, "The use of sugarcane bagasse fibres as reinforcements in composites," in *Biofiber reinforcements in composite materials*: Elsevier, 2015, pp. 525-549.
- [35] J. Kreiker, C. Andrada, M. Positieri, M. Gatani, and E. Crespo, "Study of peanut husk ashes properties to promote its use as supplementary material in cement mortars," *Revista IBRACON de Estruturas e Materiais*, vol. 7, pp. 905-912, 2014.
- [36] H.-A. S. Tohamy, B. Anis, M. A. Youssef, A. Abdallah, M. El-Sakhawy, and S. Kamel, "Preparation of eco-friendly graphene oxide from agricultural wastes for water treatment," *Desalin. Water Treat*, vol. 191, pp. 250-262, 2020.
- [37] Y. Song, J. Liu, K. Sun, and W. Xu, "Synthesis of sustainable lignin-derived mesoporous carbon for supercapacitors using a nano-sized MgO template coupled with Pluronic F127," *RSC advances*, vol. 7, no. 76, pp. 48324-48332, 2017.
- [38] B. Kishore, D. Shanmughasundaram, T. R. Penki, and N. Munichandraiah, "Coconut kernel-derived activated carbon as electrode material for electrical double-layer capacitors," *Journal of Applied Electrochemistry*, vol. 44, pp. 903-916, 2014.
- [39] Q. Xiang and J. Yu, "Graphene-based photocatalysts for hydrogen generation," *The Journal of Physical Chemistry Letters*, vol. 4, no. 5, pp. 753-759, 2013.
- [40] L. Bokobza, J.-L. Bruneel, and M. Couzi, "Raman spectra of carbon-based materials (from graphite to carbon black) and of some silicone composites," *C*, vol. 1, no. 1, pp. 77-94, 2015.
- [41] A. Ghosh *et al.*, "Structural and electrochemical properties of babassu coconut mesocarp-generated activated carbon and few-layer graphene," *Carbon*, vol. 145, pp. 175-186, 2019.
- [42] H. M. Moustafa, M. S. Mahmoud, and M. M. Nassar, "Photon-induced water splitting experimental and kinetic studies with a hydrothermally prepared TiO<sub>2</sub>-doped rGO photocatalyst," *Inorganic Chemistry Communications*, vol. 141, p. 109546, 2022.
- [43] X. Li, R. Shen, S. Ma, X. Chen, and J. Xie, "Graphene-based heterojunction photocatalysts," *Applied Surface Science*, vol. 430, pp. 53-107, 2018.
- [44] H. Liu, Y. Liu, and D. Zhu, "Chemical doping of graphene," *Journal of materials chemistry*, vol. 21, no. 10, pp. 3335-3345, 2011.
- [45] Q. Wang and K. Domen, "Particulate photocatalysts for light-driven water splitting: mechanisms, challenges, and design strategies," *Chemical Reviews*, vol. 120, no. 2, pp. 919-985, 2019.
- [46] M. Bady, "Towards Sustainable Power Generation Using Solar Chimney %J Open Access Library Journal," vol. Vol.02No.04, p. 9, Art no. 68311, doi: 10.4236/oalib.1101469, 2015.

- [47] Q. Xiang, J. Yu, and M. Jaroniec, "Enhanced photocatalytic H<sub>2</sub>-production activity of graphene-modified titania nanosheets," *Nanoscale*, vol. 3, no. 9, pp. 3670-3678, 2011.
- [48] Z. Wang *et al.*, "Crystal facets controlled synthesis of graphene@ TiO<sub>2</sub> nanocomposites by a one-pot hydrothermal process," *CrystEngComm*, vol. 14, no. 5, pp. 1687-1692, 2012.
- [49] S. Min and G. Lu, "Sites for high efficient photocatalytic hydrogen evolution on a limited-layered MoS<sub>2</sub> cocatalyst confined on graphene sheets—the role of graphene," *The Journal of Physical Chemistry C*, vol. 116, no. 48, pp. 25415-25424, 2012.
- [50] Y. Haldorai, A. Rengaraj, C. H. Kwak, Y. S. Huh, and Y.-K. Han, "Fabrication of nano TiO<sub>2</sub>@ graphene composite: Reusable photocatalyst for hydrogen production, degradation of organic and inorganic pollutants," *Synthetic metals*, vol. 198, pp. 10-18, 2014.
- [51] S. G. Babu *et al.*, "Influence of electron storing, transferring and shuttling assets of reduced graphene oxide at the interfacial copper doped TiO<sub>2</sub> p–n heterojunction for increased hydrogen production," *Nanoscale*, vol. 7, no. 17, pp. 7849-7857, 2015.
- [52] H. M. El-Bery, Y. Matsushita, and A. Abdel-moneim, "Fabrication of efficient TiO<sub>2</sub>-RGO heterojunction composites for hydrogen generation via water-splitting: Comparison between RGO, Au and Pt reduction sites," *Applied Surface Science*, vol. 423, pp. 185-196, 2017.
- [53] F. Liu *et al.*, "Near-visible-light-driven noble metal-free of reduced graphene oxide nanosheets over CeO<sub>2</sub> nanowires for hydrogen production," *Journal of the Taiwan Institute of Chemical Engineers*, vol. 107, pp. 139-151, 2020.